Imaging of Current Density and Current Pathways in Rabbit Brain During Transcranial Electrostimulation

Michael L. G. Joy,* *Member, IEEE*, Valeri P. Lebedev, and Joe S. Gati

***Abstract*— A magnetic resonance imaging (MRI) method was used for a noninvasive study of current density (CD) and current pathways (CP's) inside the skull during transcranial electrostimulation in rabbits. The transcranial impulse current directions studied were those previously used in transcranial electric treatment either sagittally or bilaterally. MRI data were collected from slices perpendicular to the direction of current application. In these slices, only the perpendicular component of the CD was measured. Computer methods for accurate topographic mapping of the main areas with high CD and for reconstruction of CP's are described.**

It was revealed that current applied on the head sagittally passed mostly through the cerebrospinal fluid in the basal brain cisternas connected in series, and through the anterior horns of the lateral ventricles, foramina of Monro, ventrocaudal part of the third ventricle, aqueductus, and fourth ventricle. Possible connections between these CP's are suggested. Bilaterally applied current passed through the brain and skull core more diffusely without concentrations in cisternas and ventricles. The results of the present study suggest an explanation for the observation that sagittally applied current more effectively stimulates brain structures with antinociceptive function and elicits more pronounced analgesic effect.

***Index Terms*—Current density (CD), magnetic resonance imaging (MRI), transcranial electrostimulation (TCES).**

I. Introduction

A. Transcranial Electostimulation (TCES) of the Brain

THERE are circumstances in life (lightning, contacts with uninsulated electric power lines) and in medical practice (electroconvulsive therapy, electronarcosis, electrosleep, electroanalgesia etc.) when electric current applied to the surface of the head could affect the brain. In order to predict the area of possible damage or to understand the mechanisms and predict the target area of the electrical stimulation for curative aims, it is necessary to determine the actual current pathways (CP's)[1] and the absolute current density (CD) inside brain tissue.

Manuscript received June 19, 1997; revised May 17, 1999. This work was supported by the National Sciences and Engineering Research Council of Canada. *Asterisk indicates corresponding author*.

*M. L. G. Joy is with the Institute of Biomedical Engineering, 4 Taddle Creek Rd., University of Toronto, Toronto, Ont. M5S 3G9, Canada (e-mail: joy@ecf.utoronto.ca).

V. P. Lebedev is with the Pavlov Institute of Physiology, Saint-Petersburg, 199034, Russia.

J. S. Gati is with the John P. Robarts Research Institute, University of Western Ontario, London, Ont. N6A 5K8, Canada.

Publisher Item Identifier S 0018-9294(99)06808-1.

[1]By CP's we mean connected regions in which we observed a current density vector with high magnitude.

Several investigations have been carried out to reveal the CD in the brain especially in connection with the problem of the target brain area of electronarcosis [1]–[3]. Most of these methods can be divided into two groups. One group uses mathematical or computer simulation of CP and CD based on (often extremely rough) approximations of the electrical characteristics of the skull and brain tissues [4]. It later became clear that the considerable level of heterogeneity and special anatomical peculiarities of brain tissue impedance are too complex for modeling [5]. In the second group of investigations an experimental approach was used for estimation of CP and CD in different parts of the brain. The first step in this approach was invasive manipulation—the insertion or implantation of special probes into the brain tissue through a hole in the skull in order to measure the electric potential difference between two brain points during transcranial current application. Current was usually calculated according to Ohm's law by means of indirect measurements of the resistance of brain tissue between electrode tips and assumptions about the CP's [6]. As is well known, interest in electronarcosis and electrosleep, elicited by transcranial electrostimulation (TCES) of the brain, diminished in the early 70's because of the practical inefficacy of both methods and presence of side effects in former. Consequently investigations of CP and CD also came to a stop. Nonetheless, several very important facts were revealed. First, only some of current applied on the skin head surface passes through the brain. Although estimates do not coincide exactly, between 10% and 45% passes through the brain [5], [6]. Second, the CD may be different in different parts of the brain. Third, the electrode position on the head affects the CP in the brain. Finally, the presence of cerebrospinal fluid (CSF) inside the cerebral ventricles is important for current propagation through the brain. Intraventricularly injected non conducting substances increased the current requirements for electroanesthesia in animals [7].

Recently, in experiments and in clinical practice, it was demonstrated [8]–[12] that TCES with specific parameters elicits profound analgesia without side effects. This type of TCES is effective only if current is applied in the sagittal direction. This nonpharmacological intervention is presently used in hospitals and outpatient clinics for arresting pain syndromes and during surgical anaesthesia to replace morphine-like analgesics. Data have been obtained which clearly indicate that this type of analgesia has a pure endorphinergic nature [13], [14]. Thus there is the possibility, that this type of TCES could activate the endorphinergic and related antinociceptive

structures located in deep brain stem structures—in the hypothalamus, midbrain, and medulla [15]–[17]. In the present study we wished to determine the magnitude of the CD in these structures without damaging the brain and skull. A newly developed noninvasive method, current density imaging (CDI), provides the unique opportunity of visualizing not only the brain structures but also, on the same image, of measuring the CD elicited by externally applied current.

B. Current Density Imaging

1) Theory: The technique of low-frequency current density imaging (LF-CDI) was first described in 1989. It has been discussed in numerous papers and abstracts by our group and by others [18]–[29]. The basic concept is to measure the magnetic field, $\mathbf{B}$, produced by a current density, $\mathbf{J}$, using the MR phase image produced by a conventional MR imaging sequence. The phase at each pixel of this image is proportional to the component of $\mathbf{B}$ parallel to the main imaging field, $\mathbf{B_0}$. By rotating the current conducting object by 90° two orthogonal components of $\mathbf{B}$, say B_x and B_y, are measured and used to compute the mutually orthogonal component, $J_z = (1/\mu_0)((\partial B_x/\partial y) - (\partial B_y/\partial x))$, of $\mathbf{J}$. The method requires no assumptions. It is exact under the assumption of a noiseless ideal MR image and a perfect 90° rotation. In practice, imperfections lead to artifacts and noise.

2) Artifacts: There are three significant sources of artifact [19] which are peculiar to LF CD images.

a) Differences in the shape of the object arising during rotation.
b) Errors in registering the B_x and B_y images.
c) Motion of the tissues which is synchronous with the MR imaging sequence.

Artifacts of the first two types are localized to those regions where the B_x and B_y images are not coincident. The magnitude of these artifacts can generally be controlled by good technique. The third type of artifact is particularly significant in *in vivo* experiments. For example during this work, the rabbits ears were observed to twitch synchronously with the 19 mA current pulses applied to its head. Since the rabbits were paralyzed, this twitch was presumably due to direct stimulation of the muscles. Motion which is synchronous with the imaging sequence leads to an artifact which appears as a high or low CD localized in the region of the image where the motion occurs. This "*twitch*" artifact does not spread out in the phase direction as do asynchronous motion artifacts in magnetic resonance imaging (MRI) such as those from respiration or blood flow. Thus all three sources of artifact in LF CDI are localized as a result of being synchronous with the entire LF CDI MRI pulse and rotation sequence.

There is also a random current "*noise*" which has been discussed elsewhere [20]. This noise is inversely proportional to signal-to-noise ratio (SNR) of the magnitude image. Since this SNR varies over the image, so does the current noise, being highest in regions, such as in air or cortical bone, where no MR signal is produced. For this reason, the current densities measured in regions with a SNR of less than some appropriate threshold (typically five) are set to zero (masked out). Nonetheless, some of the noise infiltrates the boundaries between high and low SNR regions due to the (usually) 3-pixel-square post processing filter template used to compute the required derivatives [19]. This infiltrating noise was also removed by masking out pixels adjacent to such boundaries.

C. Objectives

Using this method the aims of the present study on a live rabbit were as follows:

1) to estimate the total values of impulse current passing through the skull core via electrodes applied sagittally or bilaterally;
2) to reveal the brain regions with the highest level of the impulse CD for each position of the electrodes;
3) to follow the main CP's inside the brain by means of the three-dimensional (3-D) CDI reconstructions.

II. Methods

A. Experimental Procedure

Imaging experiments were done on four New Zealand rabbits (2.6–3.5 kg body weight), anaesthetized (Nembutal, 35 mg/kg, i.p.), paralyzed (Pavulon, 0.5 mg/kg, i.v.) and artificially ventilated and on the same rabbits after death. During the experiment additional dosages of these drugs were injected periodically if necessary. Five copper electrodes (1 cm^2 each) were inserted under the skin through small incisions and fixed by sutures. The position of electrodes was as follows: one on the forehead, two symmetrically on the both sides of the head between the eyes and ears, and one behind each ear. For the sagittal direction of current the electrode on the forehead and the pair behind ears were used. The other pair of electrodes was used for bilateral oriented current application which is ineffective for analgesia but commonly used in TCES devices for treatment of insomnia, anxiety and drug addiction [30]. The heads of rabbits were firmly fixed in plastic stereotactic frame with an angle of about 51° between the zygomatic tooth bar line and the base of the frame (see [31]). This makes the base of the brain parallel with the base of stereotactic frame. The stereotactic frame was designed to maintain the rabbits in both the horizontal (prone) and vertical position. These positions made the MRI "coronal" slices and "sagittal" slices correspond closely to those in 3-D atlas maps [31] allowing easier identification of the levels and structures [see Fig. 1(a) and (b)].

B. Correlation of the Anatomy with Magnetic Resonance Images

The task of relating points in the MR-CD image pair to points in the figures of Shek's atlas was accomplished in two steps. A "standard reference" series of MRI images of one of the rabbits was made. Using trilinear interpolation, this 3-D block of data was used to produce an interpolated image of any desired sectioning plane. The first step of the correlation process was to produce a set of interpolated images which corresponded to selected figures in an atlas of the

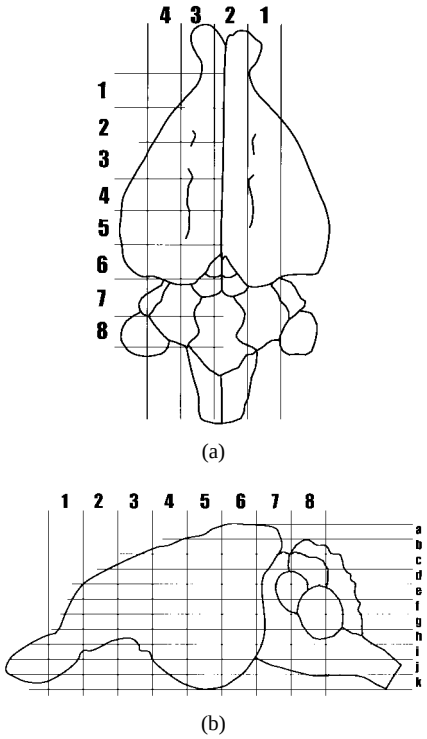

Fig. 1. (a) Dorsal contour of rabbit brain showing the levels of: the sagittal Sections 1–4 and the coronal Sections 1–8 (left). (b) Midsagittal contour of rabbit brain showing the levels of: the coronal Sections 1–8 and the interpolated horizontal Sections a–k (from top to bottom) which are three pixels (i.e., 2.34 mm) apart. Contours are drawn according to [31].

rabbit brain [31]. By this means the coordinates (left/right, posterior/anterior, superior/anterior) of any point in the figures in the atlas was established with respect to the "standard" reference series. The next step was to produce a second set of interpolated images which corresponded to the MR image in each MR-CD image pair. In the final, correlation, step the process was reversed and coordinates of any point in the MR-CD image pair was established with respect to the reference MRI series and then with respect to the figures in the atlas.

The reference MR series comprised 18 coronal and 12 sagittal slices with 0.78 mm $\times$ 0.78 mm $\times$ 3 mm voxels made on a General Electric 1.5-T Signa imager. The difference between the orientation of the reference MR images and the sections used in the atlas [31] was estimated, from the midsagittal MRI sections, to be less than 5°. The set of interpolated images corresponding to the atlas figures were spaced at the same intervals as these figures. This approach left little margin for error (beyond that associated with the finite image resolution) in the first subjective matching task. Matching of the MR-CD images to interpolated reference images was more error prone due to the lower resolution of the MR-CD images (voxel size 0.78 mm $\times$ 0.78 mm $\times$ 5 mm).

This procedure for the identification of the anatomy in the experimental MR images was verified by locating some obvious brain structures such as the olfactory bulbs, optic nerves and chiasma, ventricles, aqueduct etc. The visual identification of MR images was then verified by the coincidence of the rostro-caudal (in case of coronal images) or medio-lateral (in case of sagittal images) positions of these structures on experimental MR images and in the atlas. We estimate that the accuracy of our correlations using this method is about 1 mm in the plane of the slice.

The interpolation program was also used to create interpolated horizontal CD images from experimental sagittal and coronal CD images. These interpolated images show the CP more clearly than the experimental CD images because the imaged component of the CD lies in the interpolated image plane, not perpendicular to it. Fig. 4 is an example of such an interpolated image. Note that the effective pixels in the interpolated image are not square. In Fig. 4, for example, the pixels are 0.78×5 mm.

C. Current Density Imaging

1) Current Computations: The CDI technique used is essentially that described in [19]. The sequence described by Scott *et al*. was implemented as a multislice pulse sequence [21]. For current imaging bipolar rectangular current pulses (see [19, Fig. 2]; I =19 mA, T_c =40 ms) were used. In all cases, only one component of CD was imaged and this was always perpendicular to the imaged slice.

To make the coronal slices the rabbit was positioned vertically and the required 90° rotation was about a vertical axis. This choice minimized artifacts caused by differences in the shape of the rabbits head (due to gravity) during rotation. To make the sagittal slices the rabbit was positioned first vertically and then horizontally with rotation about a left to right axis. Here, there were certainly shape changes during the rotation which produced artifacts outside the skull. No such artifacts were found inside the skull. The rotations were accomplished using an appropriate mechanical gig, registered with the stereotactic frame. The result was verified using "scout" MR images and small adjustments made if required. The rotated images were registered on an easily visible feature inside the brain. For example, in coronal sections, the Aqueduct shown in Fig. 2, Section 7 Left side region III. Choosing the registration point inside the region of interest (ROI) minimizes the registration artifact[2] in the ROI. Four 5-mm-thick slices were made at a time and a pixel size of 0.78 mm was used throughout. Eight coronal and four sagittal sections were imaged (see Figs. 2 and 3).

The preprocessing that produces the CD image was as described elsewhere [19]. In all cases the measured current quantity was the component of CD normal to the imaged slice. A 3×3 template [20, D_3] was used for phase filtering. Since this template would allow any CD image pixel which touched a pixel which had been masked out due to low SNR[3] all such "touching" pixels were also masked out. This procedure removed the majority of "outliers" in histograms of the CD image pixel values.

2) Analysis: The current flowing orthogonal to the CD image plane through a ROI was computed by calculating the product of the pixel CD and its area and summing the result for pixels in the ROI.

[2]The registration artifact is "Artifact 2" discussed in Section I-B.

[3]Pixels with SNR less than five were masked out as described in Section I-B.

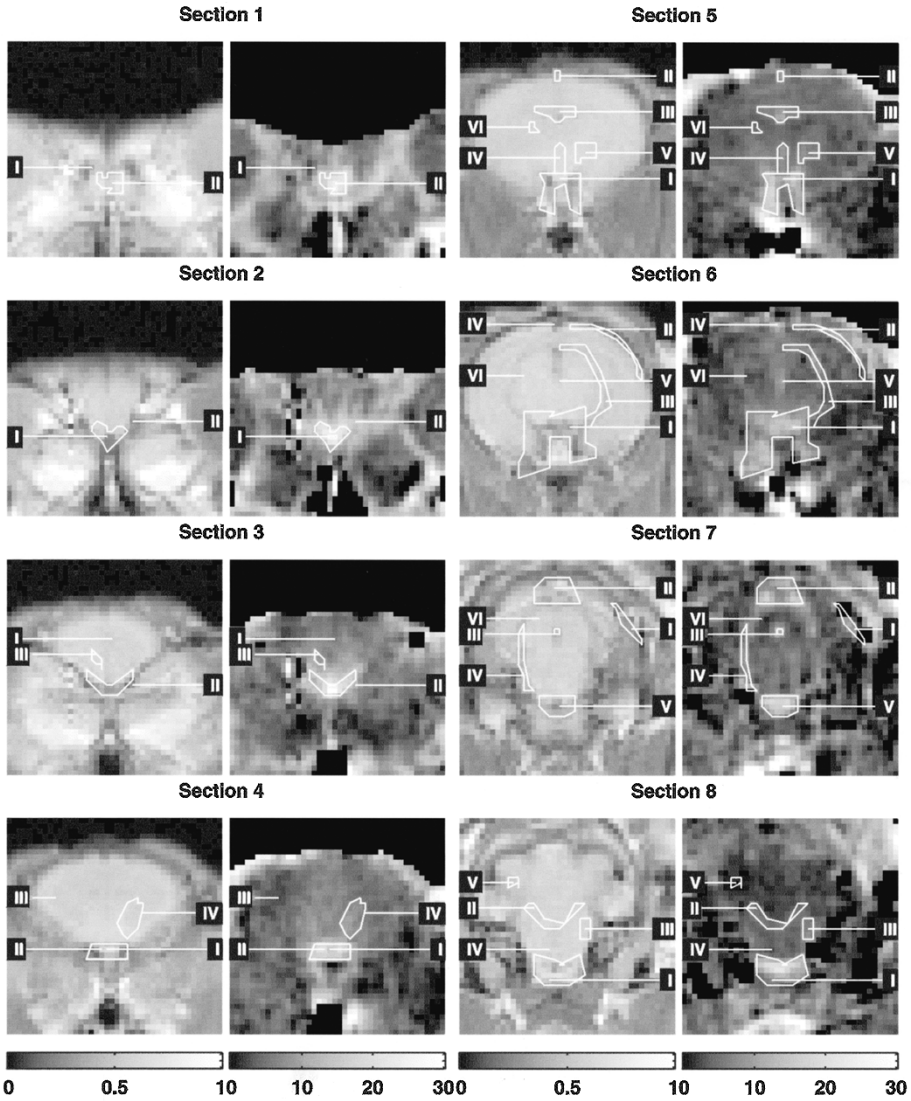

Fig. 2. MRI (left) and corresponding CD images (right) of coronal Sections 1–8. Datasets from Jun08. The current was applied sagittally. The sagittal electrodes are one on the forehead and a pair, connected electrically, one behind each ear. The datasets are from rabbit Jun08. Numbers in brackets are average CD's, in A/m^2, at the pixel or in the contour indicated. The current was applied sagittally. In the CD images, the CD scale is shown at the bottom of the figure: whitest regions correspond to 20 μA/mm^2 or more, the blackest, to 0 μA/mm^2 or negative. *Section 1:* I—Olfactory bulb (5.8); II—Space between bulbs (19.7). *Section 2:* I—Longitudinal fissure (19.4); II—Rhinal fissure (16.8). *Section 3:* I—Longitudinal fissure (5.8); II—Ventro-lateral surface, Basal cisterna (17.6); III—Lateral ventricle (10.0). *Section 4:* I—Chiasma (15.8); II—Chiasmatic cisterna (15.1); III—Centrum semiovale (2.6), IV—Lateral ventricle (7.9). *Section 5:* I—Basal cisterna (12.2); II—Longitudinal fissure (9.1); III—Region of dorsal part of Third ventricle (7.3); IV—Ventral recess of third ventricle (7.4); V—Space below pallium (6.5); VI—Thalamus (4.2). *Section 6:* I—Cisterna interpeduncularis (9.4); II—Dorso-lateral cortex (6.9); III—Space around brain stem (5.5); IV—Longitudinal fissure (15.6); V—Third ventricle (10.6); VI—Thalamus (2.3). *Section 7:* I—Dorso-lateral cortex (9.1); II—Region above colliculi (10.1); III—Aqueduct (10.6); IV—Space around midbrain (7.8); V—Cisterna pontis (11.7); VI—Periaqueductal grey (2.3). *Section 8:* I—Basal cisterna (10.8); II—Fourth ventricle (4.8); III—Lateral recess of Fourth ventricle (6.5); IV—Reticular formation (2.2); V—Cerebellar nuclei (0.6).

Several approaches to selecting ROI's were taken. To separate currents inside and outside of the skull we attempted to outline the inside of the skull (skull core). We also outlined the borders of the brain tissue attempting to exclude any intracranial spaces located peripheral to brain. The same procedure was used to outline regions of interest inside the brain (e.g., ventricles, etc.) or near the brain around the spaces which contain most of the cerebrospinal fluid (e.g., basal cisternas). In all these cases the contours were drawn on the MR image and the anatomy identified as described in Section II-B. The regions chosen were of special interest in connection with the physiological or curative effects of TCES previously described [8]–[10], [12]. In some cases contours were drawn around regions with high CD as seen on the CD image. The neighboring anatomy was subsequently identified as described in Section II-B.

III. Results

Four animals were imaged successfully. These are identified by the date of the experiment and their imaging parameters given in Table I. A complete CD experiment should comprise both coronal and sagittal MR/CD images in a single animal. From this data, the CD vectors for that animal can be confidently deduced using the assumption that the charge density remains constant $(\nabla \cdot J = 0)$. Knowledge of the CD vectors allows the CP's to be identified. We were able to

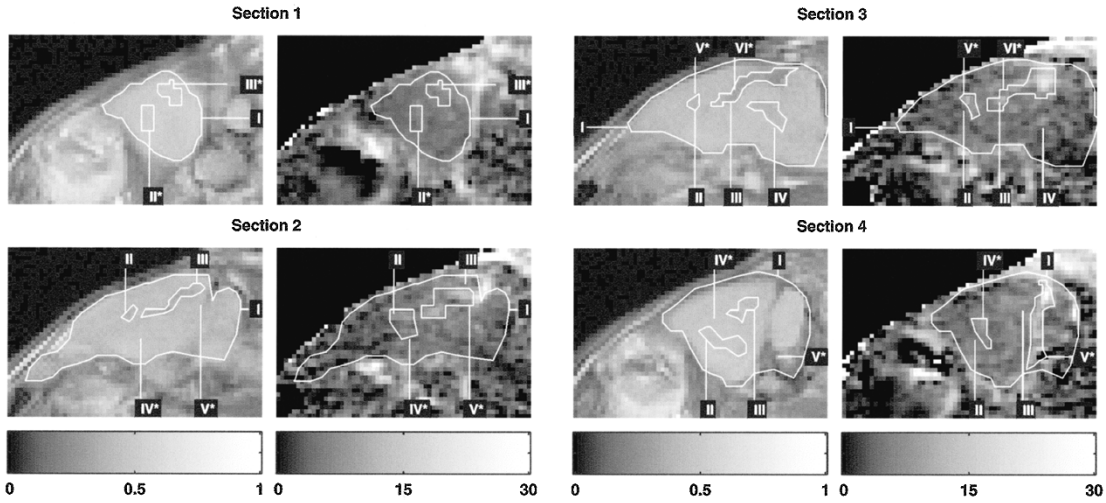

Fig. 3. MR (left) and corresponding CD (right) images of sagittal Sections 1–4. Current was applied bilaterally. The datasets from rabbit Jun08. The bilateral electrodes are at the level of Section 7 in Fig. 1, midway between eyes and ears. The annotation of this figure is different than that used in Fig. 2. The contours which were based on the MRI image (left) are drawn only on that image and not on the corresponding CD image (right), and vice versa. The Roman numerals associated with all the contours and the line which joins them to their contour is shown on both MRI and CD images. The Roman numerals with an asterisk are associated with contours drawn on the CD images to surround regions of high current. Numbers in brackets are average CD's, in A/m^2, at the pixel or in the contour indicated. *Section 1:* I—Contour of the skull core (5.5); II*—Rostral part of lateral ventricle (5.7); III*—Caudal part of lateral ventricle (7.0). *Section 2:* I—Contour of the skull core (5.3); II—Lateral ventricle (6.4); III and V*—Fissure between pallium and brain stem (9.1&8.4); IV*—Rostral part of lateral ventricle (5.8). *Section 3:* I—Contour of the skull core (5.6); II—Third ventricle, rostral (6.1); III and VI*—Fissure between pallium and brain stem (10.0&10.0); IV—Aqueductus (5.7); V*—Lateral ventricle (7.4). *Section 4:* I—Contour of the skull core (6.9); II—Lateral ventricle (5.8); III—Fissure between hemispheres and cerebellum (7.3); IV*—Rostral part of lateral ventricle (6.6); V*—Fissure between hemispheres and cerebellum (11.0). The CD scale is the same as in Fig. 2.

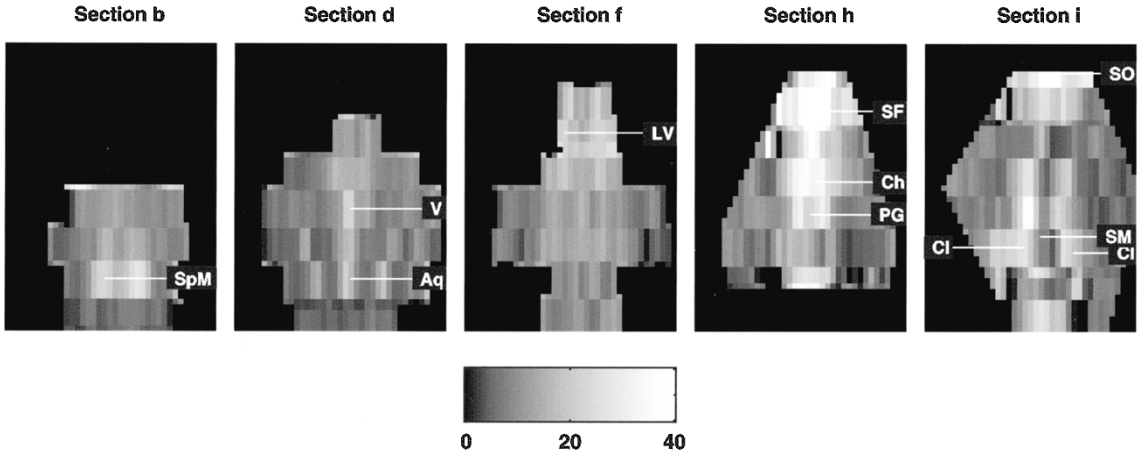

Fig. 4. Some reconstructions of CP's of sagittally applied current on horizontal sections (see Fig. 1) of the rabbit brain digitally created from coronal CD images (see Fig. 2). *Section b:* SpM-CP in space above midbrain. *Section d:* Aq and V-CP in the third ventricle and aqueductus. *Section f:* LV-CP in rostral parts of lateral ventricles. *Section h:* CP's in basal cisterna: SF—space between frontal lobes; Ch—chiasmatic cisterna; PG—position of pituitary gland. *Section i:* SO—space between opthalmic bulbs; CI—cisterna interpeduncularis. SM—space below medulla. Scale of CD is the same as in Fig. 2.

TABLE I
SUMMARY OF CDI SUBJECTS AND DATASETS OBTAINED

Subject	Applied Current Magnitude				
		Sagittal Application		Sagittal Application	
Jun01	Dead	50 mA and 10 mA	50 mA and 10 mA	10 mA	10 mA
Jun04	Alive	19 mA	Not done	Not done	19 mA
Jun08	Alive	19 mA†	Not done	19 mA	19 mA
Jun11	‡	19 mA	Not done	Not done	Not done
†	A current waveform with DC offset was also imaged.				
‡	This animal died during the imaging session.				

perform a complete CD experiment in one live animal (Jun08) with bilaterally applied current. We present this data in detail Section III-B.

In the same animal (Jun08), with sagittally applied current, we collected the sagittal but not the bilateral component of CD. In Section III-A we report detailed data from this rabbit (Jun08) and from another rabbit (Jun01) in which the missing bilateral component was measured.

Data from other datasets is reported in Section III-C. This data is much less complete than that discussed in Sections III-A and III-B, however, for the case of the sagittal component of sagittally applied current, six *approximately* identical datasets were available for comparison.

A. Current and CD in the Skull Core Elicited by Sagittally Applied Transcranial Current

1) Sagittal Components of Current Inside the Skull: Consider first the MR (left) and corresponding CD (right)

images presented in Fig. 2. Each of these images is 42 *pixels* ($\sim$33 mm) square. The levels of the MR coronal sections of the brain coincide with those indicated in Fig. 1. For each slice a contour of the region inside the skull was drawn (Skull Core). A linear regression was made between the area inside this contour and the current through it. The correlation coefficient R equaled 0.97 and the current intercept was 0.67 mA.

A more detailed description of current distribution through each section of skull core follows. In this description and in the figure captions, we have included the Roman numeral keys shown in Fig. 2. In cases where a region has been outlined, the quoted currents and CD's correspond to the pixels inside and on the contour. Otherwise they are for a single pixel.

Section 1 (Fig. 2) coincides with the transition area between olfactory bulbs I) and the frontal edge of hemispheres. At this level the highest CD's were found in the bottom part of the space between the olfactory bulbs II). This space is relatively wide in rabbits [31] and forms the most rostral part of the chain of basal cisterna [32] containing cerebro-spinal fluid (CSF). Inside the nearby brain tissue are the rostral parts of lateral ventricles. These are so narrow in rabbits ($<$ 0.7 mm) that, according to Levinger [33], they could only occasionally be filled by cast injected into the lateral ventricle. Thus the ventricle is unresolvable in the MR image.

Section 2 (Fig. 2) coincides with the frontal parts of the hemispheres. At this level the hemispheres are totally separated by sagittal longitudinal fissure with a CSF containing a cisterna of smaller diameter in bottom [32]. The diameter of the lateral ventricles at this level is about the same as in Section 1. The area with the highest CD was at the bottom of the sagittal longitudinal fissura (I). There were no areas with high CD on the dorsal and most parts of lateral surfaces of hemispheres. A single pixel with a high CD was observed near lateral surface at the level of rhinal fissure (II).

Section 3 (Fig. 2) coincides with more caudal parts of frontal hemispheres. In this section the lateral ventricles resemble slots in the dorso-ventral direction. The hemispheres begin to connect via the myelinated fibers of the corpus callosum which separates the sagittal longitudinal fissure (I) from the basal brain cisterna (II). The highest CD's (about 30 μA/mm^2) for all sections inside the skull were found in region II at the bottom between hemispheres and near their ventro-medial surface. (Section 2 has a two pixels with a comparably high CD in region I.) The CD's in the tissues, with the exception of those near the sagittal longitudinal fissure (I), was also higher in this section than in more caudal sections.

Section 4 (Fig. 2) coincides with parietal cortex, anterior part of hippocampus and optic chiasma (I). At this level the cross sectional areas of the lateral ventricles (IV) again increases. The optical chiasma (I) is surrounded by wide chiasmatic cisterna (II).

The highest CD (20 μA/mm^2) was seen in this cisterna (at the end of the bar "II"), where current flow is divided in two lateral parts by centrally located optic chiasma (I). The highest CD's in the brain were in the medial half. For example, the ventro-medial parts of right lateral ventricle (IV) located below corpus callosum carried about the same current as the chiasmatic cisterna (II). The minimal CD was in the region of centrum semiovale (III) and corona radiata where myelinated callosal fibers are predominant. There were no areas with obviously increased CD around the cortical surface or inside the longitudinal sagittal fissure.

Section 5 (Fig. 2) coincides with the middle of the hemispheres and passes through the thalamus (VI), tuber cinereum and infundibulum where the brain connects with the pituitary gland. Compared with the more rostral Section 4 the contours of ventricles have changed significantly. They are connected by means of interventricular foramina with the dorsal part of the third ventricle. The section also crosses the ventral recess of the third ventricle, just dorsal to the infundibulum. The bottom of this recess, which separates it from basal subarachnoid space, is very thin [31], [34].

In the regions outside the brain the highest CD (about 18 μA/mm^2) was seen below it to the left of the pituitary gland (in region I). The current in this area had a significant variability over the outlined region (I). This area also connects with the spaces between the lateral parts of pallium and brain stem (V) where bilateral regions of high CD were observed. An even higher CD observed near the dorsal extreme of the sagittal longitudinal fissure (II). High CD was also registered in the dorsal part of the third ventricle and adjacent medial parts of the lateral ventricles (III) and the ventral recesses of the third ventricle (IV).

The other brain tissues registered lower CD although, due to their larger area, they carried about 5 to 6 times the total current of the ventricles (III + IV). The lowest CD was found near the thalamus (VI). The low CD in the hemispheres contrasts strongly with the high currents flowing outside the dorsal part of the skull. We estimate that 1 mA was carried in the CSF around the brain and 0.25 mA in the CSF of the ventricles.

Section 6 (Fig. 2) coincides with the caudal parts of hemispheres and transition of thalamus to midbrain. The pallium is totally separated from brain stem by spaces containing CSF (III). At this level dorsal part of the third ventricle (V) connects with the aqueductus.

Again the highest CD's were outside the brain in the basal cisterna interpeduncularis (I). The outlined region (III) in the space surrounding the brain stem, clearly visible in the magnitude image, carried a CD somewhat lower than that found near the dorso-lateral surface of cortex (II) and much lower than that in the small dorsal part of the longitudinal sagittal fissure (IV) or the small caudal part of the third ventricle (V). This was the first section where an increased CD was observed near the dorso-lateral surface of cortex (II). The lowest CD was found in the thalamus (VI). As in the previous section the CD inside the skull was much less than that outside at the more dorsal surface.

Section 7 (Fig. 2) coincides with the caudal edge of pallium, the midbrain with the colliculi and aqueductus, and the cisterna pontis below the brain. As in Section 6, increased CD was observed around the both sides of the dorso-lateral cortical surface (I). A high CD was found in the region above the colliculi (II) and in the aqueductus (III). The CD in the outlined part of the lateral spaces between midbrain and pallium (IV) was elevated. The highest CD in Section 7 was observed in

the cisterna pontis (V) and the lowest CD was inside the periaqueductal grey (VI).

Section 8 (Fig. 2) coincides with cerebellum and cuts the fourth ventricle near its lateral recesses where it connects with subarachnoid space, medulla and the basal cisterna surrounding basilar artery. CD's and currents were generally lower than in Section 7. In the ventral region (I) we once again found the highest CD's and current. This current is comparable to the net current passing through the brain tissues. In the forth ventricle (II) the total current and average CD were two to four times lower. In the region of the lateral recesses of this (the fourth) ventricle (III) the average CD was slightly higher than in region II. The lowest CD's were observed in the reticular formation of medulla (IV) and in area of cerebellar nuclei (V).

2) Bilateral Components of Current Inside the Skull: We did not acquire this component of the current during the experiment reported in the previous section. In an earlier identical experiment performed on a dead rabbit (Jun01) we had two datasets with 50 mA and 10 mA applied current. For comparison with the Jun08 subject we normalized the CD's to 19 mA applied current by multiplication by $19/50$ or $19/10$, respectively.

As might be expected, transcranial current applied in the sagittal direction resulted in much more current in the sagittal than in the bilateral direction. The average bilateral component of brain CD in the midsagittal CD image Sections (2 and 3) was 0.15 μA/mm^2. This is 20 to 30 times lower than that elicited by the same current, bilaterally applied. The average CD slightly increased in the more lateral sections and was about 0.7 μA/mm^2 at Section 4 and 0.5 μA/mm^2 at Section 1. It is possible that the small increase noted in the lateral slices is related to the fact that the two caudal electrodes are located on opposite sides of the midsagittal plane.

3) Horizontal CD Interpolated Images of Sagittally Applied Currents: Horizontal CD and MR images were created by interpolation of the sagittal component data shown in Fig. 2. Horizontal interpolations of CD inside the skull are shown in Fig. 4. Skull contours from coronal MR sections were used to mask out CD and motion artifacts outside the skull. The distance between the interpolated horizontal sections is three pixels (3×0.78 mm). Note that, unlike Figs. 2 and 3, Fig. 4 shows the (rostro-caudal) CD component *in the plane* of the image not perpendicular to it. This makes the CP's more apparent in Fig. 4 than in Fig. 2.

B. Current and CD in the Skull Core Elicited by Bilaterally Applied Transcranial Current

The four sagittal MR and CD images of the bilateral component of bilaterally applied transcranial current are shown in Fig. 3. The maximal width of the rabbit brain between the most lateral poles of the hemispheres is about 30 mm with two symmetrical sides 15 mm each. This size permitted only two MR images on each side at the positions shown in Fig. 1(a). The roughly midsagittal position of Sections 2 and 3 were verified by the presence of spinal cord in the MR image.

Since the diameter of the spinal cord at the level of upper cervical segments connected with medulla is about 5 mm and the slices were also 5-mm thick, the position of Section 3 could deviate from the midsagittal plane by ± 2.5 mm. This means that Section 4 through the opposite hemisphere might be located either at the same distance from midline as Section 2 (if Section 3 were exactly at midline) or between Sections 1 and 2 or between 2 and 3 (but on the opposite side). The first option was rejected because Sections 2 and 3 were different. The latter option was rejected based on the amount of brain appearing in Section 1. The consequent assumed position is shown in Fig. 1(b).

1) Bilateral Components of Current Inside the Skull: Visual inspection of the sagittal CD images, Fig. 3, showed a rather uniform distribution of the bilaterally applied current. Increased CD was observed mainly in the space between hemispheres and cerebellum.

Two types of measurements were done. In the first we outlined regions of increased CD on the CD images. These outlines are identified by an asterisk and shown on the right and occasionally on the left in Fig. 3. The regions were then related to the atlas [31] using the method described earlier. The anatomical relationship thus discovered is noted in the caption to Fig. 3. In the second method the skull core, lateral and the third ventricles, the aqueductus and the space between pallium and brain stem were visually identified in the MR images and then outlined. These outlines are shown on the left in Fig. 3. These outline were transferred to the CD images in order to make current measurements and then removed if they overlapped the other contours. In all cases where contours would have overlapped in Fig. 3 one contour was removed, however, its annotation remains. For example in Section 2, contour IV* does not appear in the magnitude image on the left.

Data obtained by both approaches were rather similar. CD's in areas of lateral ventricles and the third ventricle were about 15% and 23%–33% higher (respectively) than average CD inside the skull. In contrast in space between hemispheres and cerebellum CD exceeded the average level by about 54%–130%. Increased CD's were observed neither in the area of aqueductus nor below the brain in area of the basal cisterna.

2) Sagittal Components of Current Inside the Skull: A Sagittal component of bilaterally applied current was also seen on some coronal sections. This component of current was significant on coronal Sections 5–7 only. These sections roughly coincide, in position and size, with the bilateral electrodes. The total thickness of three slices was about 15 mm and electrode plate was about 10-mm wide. The largest currents were observed in the lateral parts of the brain and not in the cisterna. For example in Section 5 the highest CD areas were located in the lateral parts of lateral ventricles (about 7.1–7.3 μA/mm^2). In Sections 6 and 7 higher CD's (about 8–11 μA/mm^2) were observed inside the caudal parts of lateral ventricles at the level of caudal edge of pallium. Current on the opposite sides of the brain had opposite directions. The polarity of current on each side was similar in Sections 5–7.

C. Other Datasets

The results presented in the previous Sections III-A and III-B were from six datasets and two rabbits. In this section results from the remaining datasets tabulated in Table I are discussed. These datasets are qualitatively similar to those presented

above. Since various current amplitudes were employed, the CD images were scaled by multiplication as described in Section III-A.

Images of the sagittal CD due to sagittally applied current contained more resolvable detail and were more numerous than any other type (see Table I) and are discussed in the next paragraphs. The five datasets of CD components perpendicular to the direction of current application generally had low CD's and thus statistically significant detail on the scale of a few pixels could not be resolved. The numerical data for Jun01 with 50 mA sagittally applied agreed with that for 10 mA to within stochastic error. A quantitative comparison of the three datasets (Jun01, Jun04, and Jun08) for sagittal component of bilaterally applied current was not made because the image slice orientations and positions were not the same.

Sagittal Component of Sagittally Applied Current: Immediately after the data shown in Fig. 2, for Jun08, was gathered the sequence was repeated with an asymmetric current waveform of $+18.5$ ma and -4.5 ma. When compared with Fig. 2, Sections 5 to 7 showed a higher ratio of medial to lateral CD. The high CD noted in the third ventricle (Section 5) in Fig. 2 was not seen, however, in Section 7 the high CD in the aqueduct appeared in both images. The high CD in the basal cisterna (Section 7) Fig. 2 was not as localized. Similarly, the high CD in cisterna pontis (Section 7) was missing.

The rabbit Jun01 had been dead for about one hour when the two datasets were obtained. Consequently the artifacts were greatly reduced so that regions outside the skull were credible. We were also able to image with a high (50 mA) applied current so that the CD SNR was increased. The same slice was also imaged with 10 mA and consequently appears noisier. Compared to Jun08, the position of the imaged slices are about 2.5-mm caudal and slightly oblique. A generally more medial CD concentration is observed as in Jun08 with asymmetric waveform, however, an asymmetry in the lateral CD suggests a redistribution of the CSF after death.

The images of rabbit Jun04 were severely affected by the magnetic fields due to currents in the return wires to the electrodes. These wire had not been properly positioned away from the head. The effect of this field was so severe that it reduced the intensity of the magnitude image. Since the artifact was localized, the CD's in the basal cisterna and lateral skull core are credible. The slice position and CD's in Jun04 and Jun08 were essentially identical.

Rabbits Jun11 and Jun08 had essentially identical slice position and CD's. In Slice 7, the CD patterns were more diffuse than in either Jun08 dataset. The CD in the cisterna pontis was higher than in Jun08 (with asymmetric) and more diffuse than in Fig. 2.

A linear regression for all subjects was made between the area inside skull core contour and the current through it. The correlation coefficient R equaled 0.93 and the current intercept was 0.28 mA.

IV. Discussion

The main result of the experiments presented in this paper is the demonstration of current propagation inside the skull core of the living brain by a noninvasive MR method which does not require the introduction into the brain any electrodes or probes. In the long history of TCES studies started by French physiologist S. Leduc in 1902 [35], [36], this is the first such measurement. The use of MR imagers provides the unique opportunity for quantitative measurements of CD and total current in different living tissues [18], [19], [21], [29], [37].

The accuracy of the method used has been established *in vitro* [37], [19], [20]. There are differences between the CD images recorded the different rabbits in the same rabbit with different current waveforms and between living and dead rabbits. These differences are probably significant in that they cannot be explained as artifact or stochastic noise. Factors which might explain these differences are mentioned in the results section but there is not enough data to draw firm conclusions as to their actual source.

For topographic orientation it was very helpful to be able to compare the MR and CD images of the same section (see Figs. 2 and 3). In the absence of an MRI atlas of the Rabbit brain we developed (see Methods Section B) a useful technique for correlating the MR/CD images with a histological atlas [31].

A. Fraction of Current Entering the Skull Core

The study revealed that, in rabbits, only about 14%–16% of the sagittally or bilaterally applied current passes through the skull core. It is obvious that these numbers are peculiar to rabbits because in this animal the brain occupies a relatively small part of the head. For example on coronal Section 6, (Fig. 2) where the rabbit's brain cross section is the biggest, it occupies less than 20% of the total head cross section. In contrast, the human brain occupies the most of head cross section [38]. This means that in humans during TCES the fraction of the externally applied current passing through the skull core and the brain is probably considerably higher than in the rabbit.[4]

B. Penetration of the Skull

It is very important to understand how current passes through the skull and reaches the brain. It has been suggested that current enters the skull core mainly through the large natural holes in the skull, i.e., through optic and sphenopalatine foramina. The recommendation that electrode placement be near the eyes for electrosleep or on the palate of the mouth for electroanesthesia [1], [2], [39] was based on this assumption. For sagittally applied current, the total current and average CD on either side of these foramina are about equal (see Fig. 2). Section 5 is in front of the foramina and Sections 6 and 7 are behind them). This observation demonstrates that these foramina are neither unique nor preferential for current passing to and from the skull core.

For sagittally applied current, both in subject Jun08 and over all subjects, the presence of a linear correlation of high degree between the values of total current inside the skull and areas of skull cross sections of each level suggests that

[4] In pigs, Gamba and Delpy [29] have recently reported that 22% of the applied current entered the brain.

significant current can reach the skull core throughout the whole skull surface. The results of experiments with bilaterally applied current, where rather uniform current distribution in the brain was demonstrated, also support this point of view. Possibly penetration takes place through the many small holes in the skull which contain the bone nutritional vessels. This assumption could also explain why areas with increased CD were seen near rather restricted dorso-lateral cortex areas. These areas lie below the position of temporal muscles in which high CD was usually observed.

C. Current Pathways in the Skull Core

After penetrating the skull and dura matter, current reaches the CSF (with a relatively high conductivity) and the brain tissue (with relatively low conductivity). Our data indicate that the subsequent current distribution is strongly dependant on the anatomical peculiarities of the spaces containing CSF, their interrelations with the brain structures and direction of applied current.

1) Sagittally Applied Current: The shapes of the spaces containing CSF and high CD levels were most complex for the sagittal component elicited by sagittally applied current. To better understand the CP's in sagittal direction, horizontal CD images were created and are shown in Fig. 4. This Figure shows that the CP's are located mostly in the medial part of the skull and the brain where we discovered pathways both inside and outside the brain. The pathway with highest total current passed from the ventral part of the rostral sagittal longitudinal fissure up to medulla through the chain of basal cisterna containing CSF (Fig. 4, levels d and h). At the rostral level of hemispheres some current branches to the anterior horns of the lateral ventricles and forms a second pathway (Fig. 4, level f). It seems that current can penetrate the ventro-medial walls of ventricles which are very thin at this level. Only these areas of anterior horns of the lateral ventricles are not insulated by the myelinated fibers of the corpus callosum and corona radiata which spread around its dorsal and lateral surface. In accord with this suggestion, relatively high CD was seen in coronal Sections 3 and 4 (Fig. 2) only inside the ventro-medial parts of lateral ventricles even though the dorso-lateral parts (especially in Section 4) are clearly wider.

Some current passes from the lateral ventricles through the interventricular foramina into the third ventricle. Some remains in the lateral ventricles where it spreads into their blind posterior recesses. Our data indicate that there are about three output CP's from the third ventricle. The first CP is directed caudally through the aqueductus to the forth ventricle (Fig. 4, level d). The second CP passes through the hole in the suprapineal recess where the third ventricle connects with subarachnoid space below the sagittal longitudinal fissure and above the midbrain colliculi. In this area a high level of CD was observed at Section 7 (Figs. 2 and 4, level b). This CP is probably specific to rabbits and guinea pigs because the hole in the suprapineal recess is absent in other species of mammals and humans [33]. A third CP along which part of intraventricular current passes ventro-caudally into the blind ventral recess of the third ventricle (Fig. 2, Section 5) is also possible. The bottom of the ventral recess especially in area of infundibulum is very thin [34], [31] and current could go through to the basal cisterna surrounding pituitary gland. Current passing through the fourth ventricle could also connect with the subarachnoid space via holes in lateral recesses of this ventricle (see Fig. 2, Section 8).

Hence, as was previously assumed [7], the brain's ventricular system plays an important role in the distribution of sagittally applied current. It is also very important that the ventricular CP's could have several interconnections with the CSF filled spaces outside the brain. Thus this work demonstrates that in rabbits sagittally applied current has a broad access to the medially located brain structures including hypothalamus, pituitary gland, some structures of midbrain and medulla.

2) Bilaterally Applied Current: Bilaterally applied current was distributed differently inside the rabbit's skull. The largest part of current passed bilaterally (see Results, part B). Some of it passed through the CSF containing space between the caudal edge of pallium and rostral surface of cerebellum. The main part of current penetrated the brain rather uniformly without any concentration in the brain structures and ventricles (see Fig. 3). In contrast with the sagittally applied current which had a rostro-caudal component only, it was unexpectedly demonstrated that bilaterally applied current had both bilateral and rostro-caudal components. Inside the skull the rostro-caudal component was observed in the lateral parts of the brain near the electrodes. On opposite sides this component had an opposite polarity (see Section II-B). In part, these observations of a sagittal rostro-caudal component of CD could be explained by a fringing effect at the bilateral electrodes.

In humans bilateral application of current is frequently used for TCES [30]. In our experiments in rabbits the rostro-caudal component of bilaterally applied current passed mainly through the caudal parts of lateral ventricles. In humans the lateral ventricles are more deeply located [38] than in the rabbit, and the sagittal component of bilaterally applied current might pass via the Sylvian fissures. In any case the existence of this component near the position of bilaterally applied electrodes supports our assumption that current penetrates skull bones in regions with no foramina rather diffusely.

In experimental studies and clinical trials of transcranial electroanalgesia [8], [11] it was revealed that the effects of TCES with the same electrical regime depend on the position of electrodes on the head surface. It has been demonstrated in rabbits and in humans that only sagittally applied current elicits an analgesic effect and this effect has an endorphinergic nature [13]. Our data on the differences in distribution of the sagittally and bilaterally applied currents probably provide a basis for understanding this phenomenon. The main areas in the brain which produce and release beta-endorphin are in the bottom of the third ventricle and pituitary gland [15]. It appears from our data that in the rabbit a larger fraction of applied current reaches these areas with the sagittal application than with bilateral application. In addition, other parts of the brain (e.g., periaqueductal grey) with well-known antinociceptive function [16], [17], [40], [41] are also more readily reached by sagittally applied current.

V. Conclusion

It is evident that the features of current distribution measured directly in living brain by this noninvasive MRI method substantially differ from those obtained by mathematical models and computer simulations [4], [42]. The reason for this disagreement is that the skull core contains extremely heterogeneous and anisotropic structures ignored by simple geometric approximations such as concentric sphere models. It is also evident that the current distribution demonstrated in the rabbit's skull core will differ from that inside the human skull. Therefore this noninvasive MR method should be used in human studies which require detailed information on the CD's elicited in the brain by applied currents, e.g., studies of the mechanisms of TCES effects and for improvement the arrangement of transcranial electrical treatment.

Acknowledgment

The authors wish to thank N. Siddiqi for her help with data analysis and Dr. R. M. Henkelman for his assistance with the MR imaging.

References

[1] R. H. Smith, *Electrical Anesthesia*. Springfield, MA: Thomas, 1963.
[2] A. Sances and S. J. Larson, *Electroanesthesia*. New York: Academic, 1975.
[3] D. V. Reynolds and A. E. Sjoberg, Eds., *Neuroelectric Research*. Springfield, MA: Thomas, 1971.
[4] S. Rush and D. A. Driscoll, "Current distribution in the brain from surface electrodes," *Anesth. Analg.*, vol. 47, no. 6, pp. 717–723.
[5] D. A. Driscoll and S. Rush, "Influence the cerebral spinal fluid on the current flow in the brain," in *Neuroelectric Research*, D. V. Reynolds and A. E. Sjoberg, Eds. Springfield, MA: Thomas, 1971, pp. 275–276, 1971.
[6] D. V. Reynolds, J. S. Loram, and A. E. Sjoberg, "Voltage distribution in the brain during diffusely applied electrical current in the monkey," in *Neuroelectric Research*, D. V. Reynolds and A. E. Sjoberg, Eds. Springfield, MA: Thomas, 1971, pp. 290–299.
[7] H. J. Marsoner, J. Tatsuno, and F. M. Wageneder, "Intraventriculaly injected dielectric substance to influence the current pathways," in *Neuroelectric Research*, D. V. Reynolds and A. E. Sjoberg, Eds. Springfield, MA: Thomas, 1971, pp. 277–282.
[8] V. P. Lebedev, J. S. Katznelson, V. A. Leosko, A. L. Baranovski, and G. I. Shlemis, "Anesthesia in laboratory animals achieved with combined effect of direct and impulse currents," *Fiziol. Zhurn. SSSR im. Sechenova*, vol. 68, no. 8, pp. 1120–1123, 1983.
[9] V. P. Lebedev, Ed., *New Method of Transcranial Electroanalgesia*. Leningrad: Nauka, 1987.
[10] V. P. Lebedev, "Transcranial electroanalgesia," in *Pain Syndrome*, Yu. D. Ignatov and V. A. Mokhailovich, Eds., *Medicina*, pp. 162–172, 1990.
[11] J. S. Katznelson, "Transcranial electroanalgesia in surgical anesthesia and treatment of pain syndromes," Ph.D. dissertation, Pavlov Inst. Physiol., Leningrad, U.S.S.R., 1985.
[12] S. I. Gretzov, J. S. Katznelson, G. V. Kirsanova, F. A. Gurchin, I. O. Starikova, V. P. Lebedev, and V. A. Sorokoumov, "Transcranial electroanalgesia in treatment of spondilogenic pain syndromes," *Zhurn. nevropatologii i psykhiatrii im. Korsakova*, vol. XXXX, no. 12, pp. 1800–1804, 1987.
[13] L. N. Airapetov, A. S. Zaitchik, M. S. Trukhmanov, V. P. Lebedev, J. S. Katznelson, V. A. Sorokoumov, V. G. Abisogomian, and Yu. K. Kodzaev, "Changes of the beta-endorphin levels in the brain and cerebrosrospinal fluid during transcranial electroanalgesia," *Fiziol. Zhurn. SSSR im. Sechenova*, vol. 71, no. 1, pp. 56–63, 1985.
[14] V. P. Lebedev, A. B. Savchenko, and N. V. Petryaevskaya, "Opiate mechanisms of transcranial electroanalgesia in rat and mice," *Fiziol. Zhurn. SSSR im. Sechenova*, vol. 74, no. 8, pp. 1246–1256, 1988.
[15] H. Khachaturian, M. E. Lewis, M. K.-H. Schafer, and S. J. Watson, "Anatomy of the CNS opioid systems," *Trends in Neurosci.*, vol. 8, no. 3, pp. 111–119, 1985.
[16] H. H. Fields and A. I. Basbaum, "Endogenous pain control mechanisms," in *Textbook of Pain*, P. Wall and R. Melzack, Eds. New York: Churchill Livingston, New York, 1989, pp. 206–220.
[17] J. J. Bonica, T. L. Yaksh, J. C. Liebeskind, R. N. Pechnick, and A. Depaulis, "Biochemistry and modulation of nociception and pain," in *The Management of Pain*, J. J. Bonica, Ed. Philadelphia, PA: Lea & Febiger, 1990, pp. 95–132.
[18] M. L. G. Joy, G. C. Scott, and R. M. Henkelman, "*In vivo* detection of applied electric currents by magnetic resonance imaging," *Magn. Reson. Imag.*, vol. 7, pp. 89–94, 1989.
[19] G. C. Scott, M. L. G. Joy, R. L. Armstrong, and R. M. Henkelman, "Measurement of nonuniform current density by magnetic resonance," *IEEE Trans. Med. Imag.*, vol. 10, no. 3, pp. 362–374, Sept. 1991.
[20] G. C. Scott, M. L. G. Joy, R. L. Armstrong, and R. M. Henkelman, "Sensitivity of magnetic resonance current density imaging," *J. Magn. Reson.*, vol. 97, 1992.
[21] G. Yip, M. L. G. Joy, G. C. Scott, and R. M. Henkelman, "*In vivo* current density imaging," in *Proc. 11th Annu. Meeting*, Berlin, 1992, vol. 2, p. 3917.
[22] M. L. G. Joy, V. P. Lebedev, and J. Gati, "Low frequency current density imaging in rabbits," *Ann. Biomed. Eng.*, supp1: 56, vol. 21, 1993.
[23] M. L. G. Joy, V. P. Lebedev, and J. Gati, "Current density in sections through rabbit brain," in *Proc. 2nd Meeting*, 2118 Milvia St., Berkley, CA., 1994, vol. 3, p. 1404.
[24] S. Brockstedt, M. Olsen, L. Malmgren, F. Ståhlburg, O. Henricsen, and B. R. R. Person, "An experimental system for three-dimensional mapping of electrical current distributions using a phase sensitive MR technique," in *Proc. 12th Annu. Meeting,* , Soc. Magn. Reson. Med., 1993, vol. 1, p. 351.
[25] I. Serša, O. Jarh, J. Seliger, and F. Demšar, "MR microscopy of electric currents," presented at 1st Electrochemical and Computer Science Conf., ERK'93, Slovinia, Sept. 1993.
[26] I. Sersa, O. Jarh, and F. Demsar, "Magnetic resonance microscopy of electric currents," *J. Magn. Reson., Series A*, vol. 111, pp. 93–99, 1994.
[27] I. Sersa, K. Beravs, N. F. J. Dodd, S. Zhao, and F. Demsar, "*In vivo* MRI determination of electric current density in mice tumours—A new approach for monitoring the efficiency of electrochemo tumour therapy," in *Proc. Soc. Magn. Reson., Eur. Soc. Magn. Reson. I Med. Biol.*, Nice, Aug. 1995, p. 689.
[28] B. M. Eyuboglu, R. Reddy, and J. S. Leigh Jr., "Imaging of electric current density with MR imaging," *RSNA Proc.*, 1966.
[29] H. R Gamba and D. T. Delpy, "Measurement of electrical current density distribution within the tissues of the head by magnetic resonance imaging," *Med. Biol. Eng. Comput.*, vol. 36, no. 2, pp. 165–170, Mar. 1998.
[30] M. A Patterson, L. Patterson, N. V. Flood, J. R. Winston, and S. I. Patterson, "Electrostimulation in drug and alcohol detoxification. Significance of stimulation criteria in clinical success," *Addiction Res.*, vol. 1, no. 2, pp. 130–144, 1993.
[31] J. W. Shek, G. Y. Wen, and H. M. Wishniewski, *Atlas of the Rabbit Brain and Spinal Cord*, Basel, Karger, 1986.
[32] D. Glowa, "Die subarachnoidalraume des kaninchengehirns," *Anat. Anz.*, vol. 136, nos. 1–2, pp. 17–23, 1974.
[33] I. M. Levinger, "Special features of the rabbit cerebroventricular system, studied by casting method," *J. Anat.*, vol. 109, no. 3, pp. 527–533, 1971.
[34] I. Urban and P. Richard, "A stereotaxic atlas of the new zealand rabbit's brain," 1972.
[35] S. Leduc, "Production du sommeil et de l'anesthésie général et local par le courants electriques," *C. R. Acad. Sci.*, vol. 135, pp. 199–200, 1902.
[36] S. Leduc, "L'inhibition cérébral electrique chez l'homme," *Arch. d'Electricité Medicale*, vol. 120, pp. 769–775, 1902.
[37] J. D. M. Thompson, M. L. G. Joy, and R. M. Henkelman, "Current density imaging in rabbit head and chest," in *10th Annual Meeting, Works in Progress*. New York, Soc. Magn. Reson. Med., 1991, p. 1274.
[38] M. Wagner and T. L. Lowson, *Segmental Anatomy. Applications to Clinical Medicine*. New York: MacMillan, 1982.
[39] P. Philip, J. Demotes, M. Bourgeous, and J. D. Vincent, "Efficiency of transcranial electrostimulation on anxiety and insomnia symptoms during washout period in depressed patients, double-blind study," *Biol. Psych.*, vol. 29, no. 5, pp. 451–456, 1991.
[40] M. F. Roizen, "Reduced anaesthetic requirements after electrical stimulation of the periaqueductal grey matter," *Anesthesiol.*, vol. 62, no. 2, pp. 120–123, 1985.
[41] K. Kumar, B. M. Wyant, and R. Nath, "Deep brain stimulation for control intractable pain in humans, present and future: A ten-year follow-up," *Neurosurg.*, vol. 26, no. 5, pp. 771–781, 1990.
[42] E. J. Vresilovic, S. R. Pollack, and C. T. Brihton, "A generalized theoretical approach to the determination of local field parameters during capacitively coupled electrical stimulation *in vivo*," *Trans. Bioelectr. Repair Growth Soc.*, vol. 10, p. 2, 1982.

Michael L. G. Joy (M'83) received the B.Sc. degree in physics in 1963 and the Ph.D. degree in electrical engineering in 1970, from the University of Toronto, Toronto, Ont., Canada.

Since 1970 he has been cross appointed between what is now the Institute of Biomaterials an Bioengineering and the Department of Electrical and Computer Engineering where he recently served a term as the Associate Chair for the Undergraduate Programs in electrical engineering and computer engineering. His research has always been in the field of medical imaging and has ranged from building gamma ray cameras and coded aperture imaging to magnetic resonance imaging. His goal has been to develop new ways to image.

Valeri P. Lebedev was born in Leningrad, USSR (now St. Petersburg, Russia) in 1933. He received the M.D. degree from the First Leningradian Medical School, Leningrad, Russia, in 1956 and the Ph.D. degree in neurophysiology in 1959. He received the Dr. of Sciences in Neurophysiology degree in 1998.

He worked in the Department of Pharmacology as an Associate Professor. Since 1966, he has worked in the Pavlov Institute of Physiology, Russian Academy of Sciences, Saint-Petersburg and is currently a Professor and head of the Electroanelgesia research group, Russian Academy of Sciences. He investigates, in collaboration with foreign researchers and clinicians and the mechanisms and efficiency of the new electrical regime for transcranial stimulation of the brain in animals and humans.

Joe S. Gati received the B.Sc. degree in physics and the M.Sc. degree medical biophysics from the University of Western Ontario, London, Ont., Canada.

He is currently the Operations Manager at The Laboratory for Functional Magnetic Resonance Research in the John P. Robarts Research Institute, London, Ont., Canada. He is involved in the development and implementation of acquisition schemes for high spatial and temporal resolution functional MRI applications at four tesla.